

Chapter 6

Spaceborne SAR Antennas for Earth Science

Yunjin Kim and Rolando L. Jordan

6.1 Introduction

Before the development of the first synthetic aperture radar (SAR) antenna flown in space, Jet Propulsion Laboratory (JPL) was involved in an aircraft radar program to image the Earth surface for various science applications. This radar was flown on a Convair CV-990 aircraft with the antenna attached to one of the baggage doors of the airplane. The antenna was a planar array with eight radiating elements operating at 1215 MHz and had dual-polarization capability. This system was important because it provided SAR data to prove that SAR could image ocean waves giving both the direction of wave propagation and its wavelength. These observations led to the incorporation of SAR on the Seasat spacecraft that was the first radar used to make science observations from space [1]. The development of the Seasat antenna was significant because of the unique challenges that its development required. The antenna area required was significantly larger than other similar antennas built for aircraft systems. In addition, the antenna was required to operate in a vacuum over a wide temperature range without its surface deforming significantly from out of plane, and the mass of the antenna was limited to less than 100 kg. A picture of the Seasat-A system is shown in Fig. 6-1.

Ball Aerospace developed both engineering and flight models of the Seasat antenna. The engineering model was used to verify the performance of the antenna, and the flight model was flown on the Seasat platform. Following the success of the Seasat SAR system, the first of the Shuttle Imaging Radar (SIR)

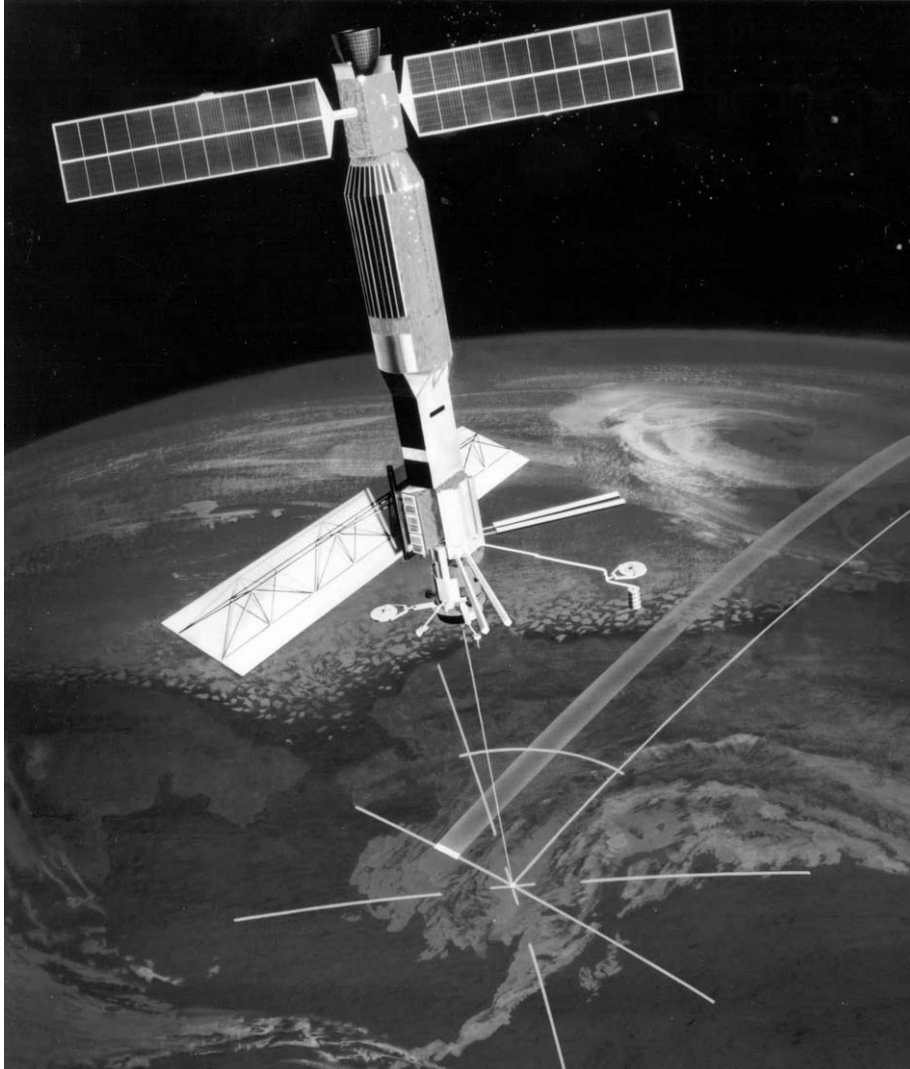


Fig. 6-1. Seasat synthetic aperture radar. The Seasat antenna is the large deployed structure near the bottom of the spacecraft.

systems, SIR-A, was flown in the Shuttle in 1981. This radar used the leftover hardware from Seasat. In particular, the antenna system used seven Seasat engineering model panels. This antenna was again flown on the Shuttle as part of the SIR-B radar instrument [2].

The SIR-C was launched on the Space Shuttle Endeavour for two 10-day missions in the spring and fall of 1994 [3]. During these two missions, radar data from more than 300 sites around the Earth were collected to investigate the

use of fully polarimetric, multi-frequency SAR to understand global environmental changes. The SIR-C antenna represents major advances in radar technology to obtain fully polarimetric SAR data from space [4]. In order to measure the weak cross-polarization signal, the SIR-C antenna must be efficient. Using transmit/receive (T/R) modules close to radiating microstrip patches, the antenna loss is reduced, and an extremely high-power transmitter is avoided. By adding a phase shifter to each T/R module, the SIR-C antenna beam can be electronically steered. Using this capability, various advanced SAR technologies (phase beam broadening, the scan mode synthetic aperture radar (ScanSAR), and spotlight operation) were tested in space. The SIR-C antenna is the world's first civilian phase-array SAR antenna in space. The SIR-C antenna was manufactured by Ball Aerospace with close technical collaboration from JPL.

The Shuttle Radar Topography Mission (SRTM), a joint project between the United States National Imagery and Mapping Agency (NIMA) and the National Aeronautics and Space Administration (NASA), used modified hardware from the C-band radar of the SIR-C system, with a 62-m long mast and a second antenna to form a single pass interferometer [5,6] (see Fig. 6-2).



Fig. 6-2. SIR-C and SRTM phase array antennas. The SIR-C L-band (composed of larger upper panels) and C-band (smaller lower panels) phase-array antennas are shown in upper left. The SIR-C C-band antenna was used for SRTM with the outboard C-band antenna (lower left) to form a SAR interferometer.

The second antenna, known as the outboard antenna, is a receive-only phase array antenna. SRTM was the first spaceborne implementation of a single pass interferometer. It was launched in February 2000 on the Space Shuttle Endeavour. The SRTM mission acquired digital topographic data of the globe between 60 deg north and south latitudes during one 11-day Shuttle mission. The SRTM implemented the ScanSAR operation for a large swath required for the global coverage during eleven days. The major challenge of the SRTM antennas was the phase stability to form a SAR interferometer. The SRTM mission was successfully implemented, and JPL finished the processing of the global digital elevation model (DEM) data in January 2003.

Any future SAR antenna must reduce its weight and stowed volume to lower the mission cost and to enable a larger antenna required at higher orbits such as medium Earth orbit (MEO) and geosynchronous Earth orbit (GEO). Both mechanically deployable and inflatable technologies can provide a light-weight antenna structure. High efficiency, light-weight, miniaturized transmit/receive (T/R) modules are being developed for future SAR missions. These new technologies will revolutionize the future science observations. As an example, NASA formed the Solid Earth Sciences Working Group (SESWG) to formulate a scientific observational program for NASA in the next decade [7]. The SESWG final report calls for its highest priority to be “InSAR (Interferometric SAR) everywhere, all the time” to make vector surface deformation measurements of millimeter-scale accuracy over wide areas using repeat-pass SAR interferometry. New antenna technologies are required to enable continuous observations of the Earth surface for understanding global environmental changes and mitigating natural hazards.

6.2 Characteristics of Spaceborne Earth Science SAR Antennas

We start this section with the basic principles of SAR to provide SAR antenna design requirements. A conventional SAR is a two-dimensional imaging instrument that uses the time delay and the Doppler information to achieve the desired range and azimuth resolutions [8–11]. That is, the time delay between the echoes that are back-scattered from different surface elements is used to separate them in the range (cross-track) direction, and the Doppler information is used to separate surface pixels in the azimuth (along-track) direction.

First, we discuss the antenna size requirement. The antenna width (W) is determined by the illuminated swath size. The swath size can be specified by the minimum (θ_L^{\min}) and the maximum (θ_L^{\max}) look angles. The look angle is defined as the angle between the spacecraft nadir direction and the radar beam at the spacecraft. The minimum look angle is usually determined by science

applications and the ground topography to avoid the layover problem. In order to illuminate the desired swath, the cross-track beam width (θ_{BW}^C) satisfies

$$\theta_{BW}^C = \kappa_c \frac{\lambda}{W} = \theta_L^{\max} - \theta_L^{\min} \quad (6.2-1)$$

where κ_c is the broadening factor determined by the antenna tapering. The look angle should be calculated including the Earth curvature effect. Assuming that Earth is a sphere with the radius R , the actual curved swath can be calculated using Eqs. (6.2-2), (6.2-3), and (6.2-4). The angles shown in Fig. 6-3 are related by

$$\frac{\sin(\theta_L)}{\sin(\theta_I)} = \frac{R}{R+H} \quad (6.2-2)$$

where θ_I is the incidence angle and H is the platform altitude. The angle denoted by θ_E (see Fig. 6-3) is defined as

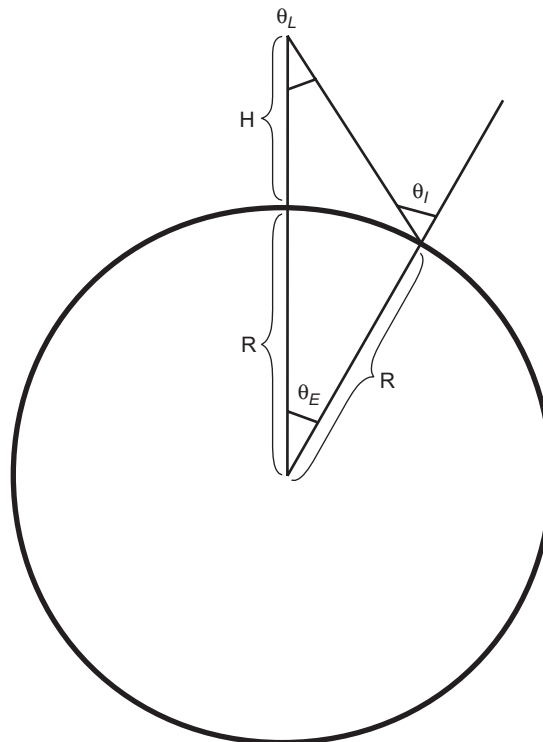


Fig. 6-3. Definition of θ_L (look angle), θ_I (incidence angle), and θ_E . The platform altitude and the Earth radius are denoted by H and R , respectively.

$$\theta_I = \theta_L + \theta_E \quad (6.2-3)$$

Then, the curved swath (S) is given by

$$S = R(\theta_E^{\max} - \theta_E^{\min}) \quad (6.2-4)$$

where the angles θ_E^{\min} and θ_E^{\max} are associated with the corresponding look angles θ_L^{\min} and θ_L^{\max} . As an example, we will determine the antenna width when the platform altitude is 700 km, the desired swath is 100 km, and the minimum incidence angle is specified to be 20 deg. The Earth radius is 6378 km. For the minimum incidence angle, the minimum look angle is calculated using Eq. (6.2-2) to be 17.95 deg. Therefore, $\theta_E^{\min} = 20 - 17.95 = 2.05$ deg using Eq. (6.2-3). Then, θ_E^{\max} is calculated to be 2.95 deg by solving Eq. (6.2-4) for $S = 100$ km. Using Eqs. (6.2-2) and (6.2-3), the maximum look angle is 24.84 deg, and the antenna beamwidth becomes 6.89 deg. For L-band SAR with the center wavelength of 0.24 m, the antenna length must be 2 m (assuming $\kappa_c = 1$) to illuminate a 100-km swath at the altitude of 700 km.

We would like to emphasize that the antenna width can be larger than the one defined in Eq. (6.2-1) since the swath does not have to be defined by the 3-dB antenna beamwidth as long as a SAR instrument provides the adequate signal-to-noise ratio (SNR) over the entire swath. When a much larger swath is required, a ScanSAR operation can be implemented. The ScanSAR operation achieves a larger swath by moving an antenna beam electronically in a pre-determined sequence in the cross-track direction. However, this increase in the swath size causes degradation of the azimuth resolution by reducing the observation time.

The SAR azimuth resolution depends on the observation time of an imaged pixel. As a SAR instrument “sees” a pixel longer, the azimuth resolution increases. That is, the SAR synthesizes a longer antenna by observing a pixel longer to increase the resolution. The azimuth resolution (Δ_a) is given by

$$\Delta_a = L/2 \quad (6.2-5)$$

where L is the length of a SAR antenna. Equation (6.2-5) indicates that the antenna length must be smaller for better azimuth resolution. Notice also that Eq. (6.2-5) is independent of the SAR wavelength and the platform altitude. For example, if the antenna length is 14 m, the best azimuth resolution that can be accomplished is 7 m, unless a spotlight operation is implemented.

A SAR instrument is designed to transmit pulses periodically and collect the returned signals. This periodic sampling frequency is known as pulse repetition frequency (PRF). Since a SAR must sample the Doppler information

correctly without aliasing, the PRF must satisfy the Nyquist sampling requirement. This condition is given by

$$PRF \geq \frac{2V}{L} \quad (6.2-6)$$

where V is the spacecraft velocity. Due to this periodic sampling, SAR suffers two artifacts known as range and azimuth ambiguities. For a spaceborne SAR instrument, the PRF is high (>1000 Hz) since a spacecraft moves fast (7.5 km/s at low Earth orbit (LEO)). Since the altitude is high and the illuminated ground area is large, many transmit pulses are in the air simultaneously. Therefore, there is a chance that several successive pulses, after being reflected from different pixels on the ground, can arrive at a SAR antenna at the same time. This artifact unique to SAR is known as the range ambiguity. In order to make sure that the range ambiguity signals are not from the half-power beamwidth (HPBW), the PRF must satisfy the condition given by

$$PRF < \frac{cW}{2\rho_m \lambda \tan(\theta_I)} \quad (6.2-7)$$

where ρ_m is the slant range between a SAR antenna and the middle point of the swath and c is the speed of light. Here, we also assume that $\kappa_c = 1$. When the condition of Eq. (6.2-7) is satisfied, the range ambiguity signal is much smaller than the desired return signal. Using Eqs. (6.2-6) and (6.2-7), a condition known as the minimum SAR antenna size can be derived as

$$LW > \frac{4V\rho_m \lambda \tan(\theta_I)}{c} \quad (6.2-8)$$

However, this condition shown in Eq. (6.2-8) is only required if the entire illuminated area (defined by the 3-dB beamwidth) is used for the SAR imaging swath. If a radar designer wants to use only part of the swath for SAR imaging, the condition shown in Eq. (6.2-8) does not have to be satisfied. Interested readers should read detailed descriptions of these SAR artifacts in [8–11].

Another condition that a SAR antenna must satisfy is that the received signal must be strong enough to provide the sufficient SNR. This condition provides the requirement on the antenna size, the antenna efficiency, the peak transmit power, and the pulse length. The condition can be derived from the radar equation given by

$$P_r = \frac{P_t G_t}{4\pi\rho^2} A_I \sigma_0 \frac{\lambda^2 G_r}{(4\pi\rho)^2} \quad (6.2-9)$$

where P_r is the radar receive power, P_t is the radar transmit power, G_t is the transmit antenna gain, ρ is the slant range, A_I is the illuminated ground area, σ_0 is the backscattering cross section, and G_r is the receive antenna gain. We explicitly show different transmit and receive antenna gains because two different antennas may be used for SAR polarimetry and SAR interferometry to be discussed later in this chapter. The illuminated ground area (A_I), under the pulse-limited condition, can be written as

$$A_I = \rho \frac{\lambda}{L} \frac{c\tau_p}{2\sin(\theta_I)} \quad (6.2-10)$$

where τ_p is the pulse length. Equation (6.2-10) is true for the pulse-limited condition where the illuminated ground (in the range direction) at any instance is limited by the pulse length instead of the antenna illuminated area. Then, the radar equation becomes

$$P_r = \frac{P_t G_t}{4\pi\rho^2} \rho \frac{\lambda}{L} \frac{c\tau_p}{2\sin(\theta_I)} \sigma_0 \frac{\lambda^2 G_r}{(4\pi\rho)^2} \quad (6.2-11)$$

The gain of a SAR antenna is related to the antenna directivity (D) as

$$G = \eta D \quad (6.2-12)$$

where η is the antenna radiation efficiency. The directivity is given by

$$D = \frac{4\pi}{\theta_r \theta_a} \approx \frac{4\pi LW}{\lambda^2} \approx \frac{4\pi A}{\lambda^2} \quad (6.2-13)$$

where θ_r and θ_a are 3-dB beamwidths in the range and azimuth directions, respectively, and A is the antenna area. From Eq. (6.2-11), in order to receive radar echoes with the sufficient SNR, the antenna area must be large, and the efficiency must be high. In addition, the peak transmit power and the pulse length are critical SAR design parameters. When a SAR instrument is designed, all four parameters (antenna area, antenna efficiency, peak transmit power, and pulse length) must be considered simultaneously to provide the sufficient SNR within available technologies. The product of the peak transmit power and the transmit gain is known as equivalent isotropically radiated power (EIRP). If the transmit power is required to be extremely high, available transmitter technologies must be considered carefully, and it is important to design the thermal management system to remove the heat properly from the radar system. Another factor to be considered for a phased-array antenna is the antenna

receiver noise figure since an excellent low-noise receiver can increase the SNR.

The antenna sidelobe is related to SAR image artifacts known as the range ambiguity and the azimuth ambiguity. As an example, the two-way antenna pattern (Φ) of a uniformly excited (no tapering) phase array is given by

$$\Phi(\theta_{RA}) = \left[\frac{\sin\left(\frac{kW}{2} \sin\theta_{RA}\right)}{\frac{kW}{2} \sin\theta_{RA}} \right]^4 \quad (6.2-14)$$

where θ_{RA} is the range angle in the cross-track direction. The range ambiguity signals can be calculated from the condition given by

$$\Delta\rho(n) = \frac{n}{2} \frac{c}{PRF} \quad (6.2-15)$$

where $\Delta\rho(n)$ is the range difference between the desired signal and the ambiguity signal, and n is a non-zero integer. For a given slant range ρ , the range ambiguity signals have the slant range defined by

$$\rho_{RA}(n) = \rho + \Delta\rho(n) \quad (6.2-16)$$

where $\rho_{RA}(n)$ is the range ambiguous slant range. For each $\rho_{RA}(n)$, the corresponding look angle can be calculated using

$$\cos(\theta_L(n)) = \frac{H^2 + \rho_{RA}^2(n) + 2RH}{2\rho_{RA}(n)(R+H)} \quad (6.2-17)$$

If the antenna is mechanically titled and the boresight is given by θ_B , the antenna angles ($\theta_A(n)$) corresponding to the ambiguities are given by

$$\theta_A(n) = \theta_L(n) - \theta_B \quad (6.2-18)$$

As an example, we consider a spaceborne platform at 800 km with an L-band (center wavelength = 0.24 m) antenna. If the antenna width is 2.5 m, and the PRF is 1350 Hz, the range ambiguities corresponding to the antenna boresight are shown in Fig. 6-4.

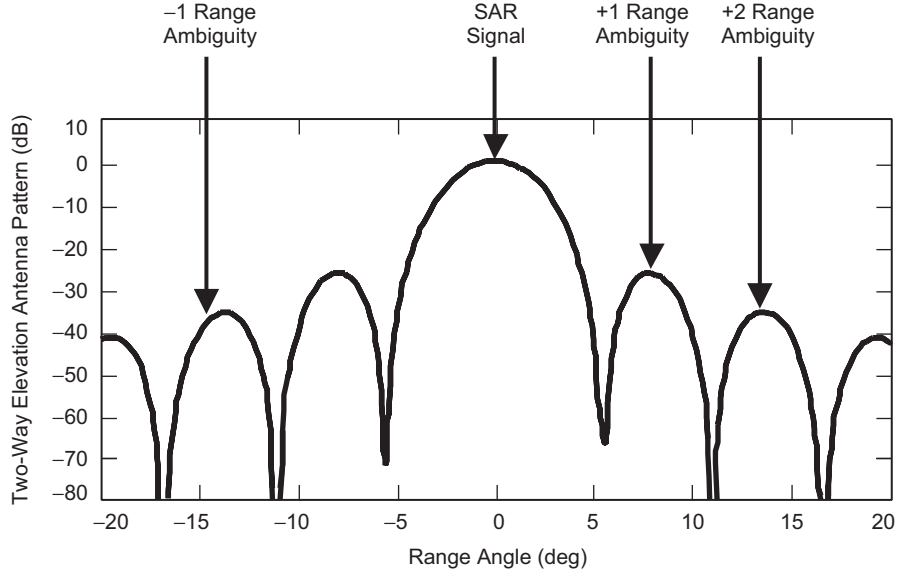


Fig. 6-4. Two-way antenna pattern with three range ambiguities. As PRF becomes lower, the range ambiguity signals move away from the antenna boresight; therefore, the overall range ambiguity is reduced. Notice that the ambiguity signals are separated by unequal angles in the range direction.

The range ambiguity ratio (RAR) can be calculated using

$$RAR = \frac{\sum_{n \neq 0} \frac{G_t(\theta_A(n))G_r(\theta_A(n))}{\rho_{RA}^3(n) \sin(\theta_I(n))}}{\frac{G_t(\theta_A(0))G_r(\theta_A(0))}{\rho^3 \sin(\theta_I)}} \quad (6.2-19)$$

Equation (6.2-19) assumes that the backscattering cross section is independent of incidence angle. From Eq. (6.2-19), it is clear that the antenna pattern must be controlled to limit the range ambiguity contamination.

The azimuth ambiguity contamination is caused by aliased signals due to a periodic sampling of Doppler information. The Doppler frequency (f_D) is given by

$$f_D = \frac{2V \sin(\theta_{AZ})}{\lambda} \quad (6.2-20)$$

where θ_{AZ} is the azimuth angle in the along track direction. The azimuth ambiguity signals can be expressed as

$$f_D \pm n \text{ PRF} = \frac{2V \sin(\theta_{AZ}(n))}{\lambda} \quad (6.2-21)$$

where n is a non-zero integer. Since the antenna pattern is very narrow in the azimuth direction, we assume that the backscattering cross section, the slant range, and the incidence angle are constant. Under this assumption, the azimuth ambiguity ratio (AAR) is given by

$$AAR = \frac{\sum_{n \neq 0} \int_{PB} G_t(\theta_{AZ}(n)) G_r(\theta_{AZ}(n)) d\theta_{AZ}(n)}{\int_{PB} G_t(\theta_{AZ}(0)) G_r(\theta_{AZ}(0)) d\theta_{AZ}(0)} \quad (6.2-22)$$

where PB is the Doppler processing bandwidth.

As an example, the azimuth ambiguities of a low-Earth orbiting (orbiting velocity = 7.5 km/s) L-band SAR are shown in Fig. 6-5. The processing bandwidth identified by vertical lines is selected for the 10-m azimuth resolution. The antenna length and the PRF are 12 m and 1350 Hz, respectively. The desired Doppler signal is the area under the two-way antenna pattern over the processing bandwidth. The aliased azimuth ambiguity signals are shifted by the integer multiple of PRF.

The impulse response of a pixel in the range direction depends on the frequency transfer function of a SAR system. Therefore, the antenna frequency

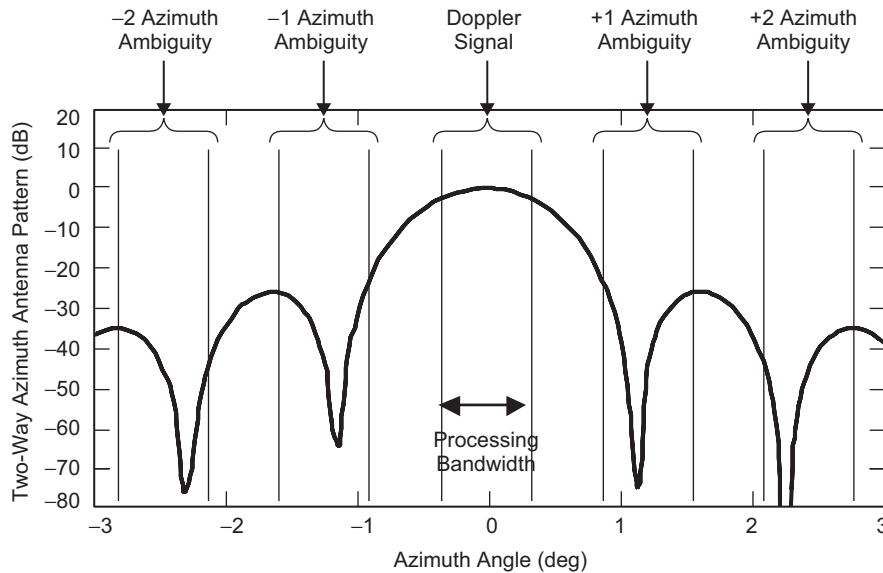


Fig. 6-5. Two-way antenna pattern with four azimuth ambiguities. As PRF increases, the azimuth ambiguities move away from the Doppler signal; therefore, the total azimuth ambiguity decreases.

response must satisfy the requirement on the integrated sidelobe level. The main product of a traditional SAR instrument is the calibrated backscattering cross section (σ_0). Since SAR measures the received power, one must derive σ_0 using the radar equation shown in Eq. (6.2-9). One of the critical components of this calibration is the antenna pattern. Therefore, the precise measurement of an antenna pattern is required before the satellite is launched. For polarimetric SAR, the cross talk between different polarization channels must be estimated and removed. A polarimetric antenna with sufficient polarization isolation will reduce the calibration burden to remove the cross talk contamination caused mainly by an antenna.

To complete the discussion on a SAR system, we provide a brief description of a SAR hardware system. A simplified radar block diagram is shown in Fig. 6-6 to illustrate the SAR hardware configuration. Received SAR signals must be coherent over the synthetic aperture length. To ensure the coherence, all radar elements are synchronized by timing signals derived from a stable local oscillator. A PRF timing signal triggers the generation of a low-frequency waveform signal. A usual waveform is a linear frequency modulation (FM) signal that is also known as a chirp signal. The bandwidth of the waveform determines the range resolution. A linear FM signal can be generated

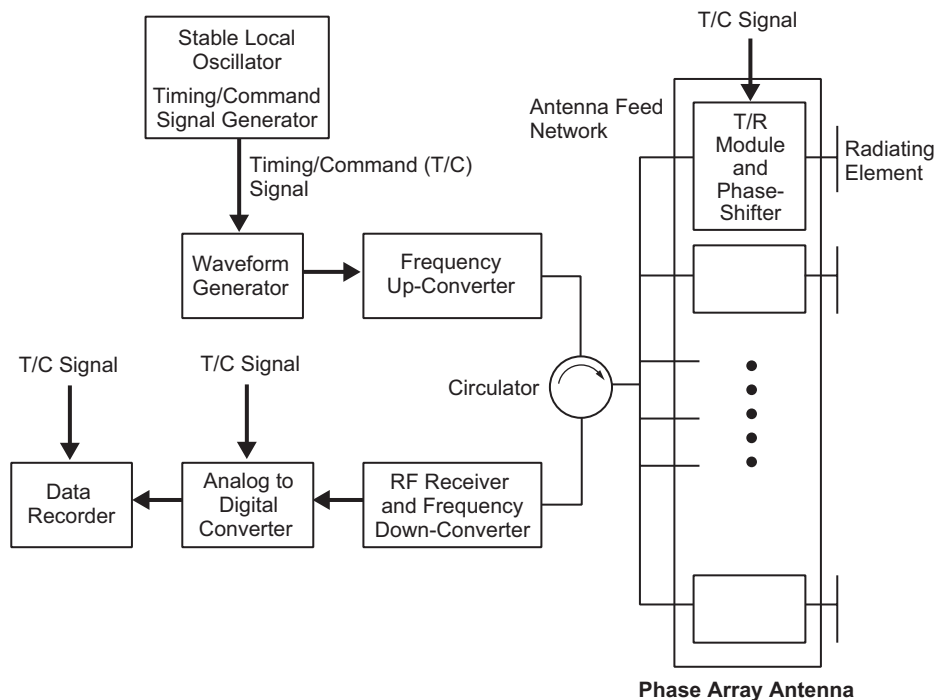


Fig. 6-6. SAR hardware block diagram including radar electronics and a phase array antenna.

using a numerically controlled oscillator (NCO). The center frequency of the waveform must be moved to the desired RF frequency using a frequency up-converter. The frequency conversion is typically performed using a mixer and a filter. An amplifier may be needed to increase the signal strength before the RF radar signal is delivered to an antenna through an antenna feed network. If the antenna contains no amplifiers, a high power transmitter such as a traveling wave tube amplifier (TWTA) is required to amplify the signal before it is delivered to the antenna. The feed network is composed of power dividers and RF cables or waveguides. For a phased-array antenna, a low-power RF signal is delivered to the antenna, and the signal is amplified and phase-shifted by transmit/receive (T/R) modules and phase shifters. This phase-shift operation is performed to send the radar signal to the desired direction. After the radar signal is reflected from the ground, the return signal is properly amplified by T/R modules. Then, the return signals are combined by the antenna feed network, and the combined signal is amplified by a low-noise amplifier (LNA). This signal is down-converted before it is digitized by an analog-to-digital converter (ADC). The digitized signal is stored at a data recorder to be processed later.

For a phased-array antenna, a T/R module is the most important element. A T/R module is composed of the control circuit, a high-power amplifier (for transmit), an LNA (for receive), and a duplexer. A duplexer can be a circulator or a T/R switch. An important factor in the T/R module design is the power efficiency (from direct current (DC) to RF conversion) and the thermal management. The receiver amplifier performance is characterized by the noise figure. A duplexer must provide the high isolation between transmit and receive paths and the insertion loss must be low. The uniformity of T/R modules is essential for producing a high gain antenna (HGA) pattern. Therefore, the root mean square (rms) amplitude and phase errors of T/R modules must be minimized. Especially, a linear phase error over the entire antenna length can cause a beam-pointing error. Since many T/R modules are required for a phased-array antenna, the cost and the weight of a T/R module is a significant design factor. The packaging and assembly of a T/R module must be simplified to produce an affordable T/R module. A typical phase shifter uses several RF switches to produce variable phase changes. For example, a four-bit phase shifter has the phase changes of 22.5, 45, 90, and 180 deg. Low insertion loss is the most important factor in selecting a phase shifter.

6.3 Seasat, SIR-A, and SIR-B Spaceborne Antennas

The Seasat SAR was the first imaging radar designed to acquire data from space to be used for scientific purposes. The Seasat satellite was a near-polar orbital platform at an 800-km altitude. The SAR instrument was designed to acquire radar backscatter data over a 100-km swath at a resolution of 25 m. The

imagery was a pictorial representation of the radar backscatter of the surface of the Earth in a map-like representation. The development of the Seasat SAR antenna was significant because it provided enabling technologies for a series of follow-on SAR systems that were flown on the Space Shuttle. Lessons learned during the Seasat SAR development phase and the analysis of the science data acquired had a large impact on the development of the later spaceborne SAR systems.

The Seasat SAR system, as shown in Fig. 6-7, includes a planar array antenna excited by 1-kW peak power transmitter. Upon reception of the return echo by the antenna, the signal was amplified by a receiver and up-converted to the downlink S-band frequency. The up-converted receiver output was then combined with timing and frequencies derived from the local oscillator for the synchronous demodulation on the ground. The data was recorded in digital format on the ground for later processing. The system was designed to acquire the 100-km swath for 10 minutes duration. This was the nominal duration for which Seasat was in view of any ground station while in orbit. The resulting data from a single pass covers an area of 4000 km by 100 km on the ground.

The Seasat SAR antenna was a 10.74-m (along-track direction) by 2.16-m (cross-track direction) planar array antenna. The antenna was composed of eight microstrip antenna panels, each 1.34 m in length and 2.16 m in width. As shown in Fig. 6-8, these panels were mounted on a composite truss structure that was deployed once in orbit. The deployed antenna was configured to fly with the long dimension along the spacecraft velocity vector, and the antenna

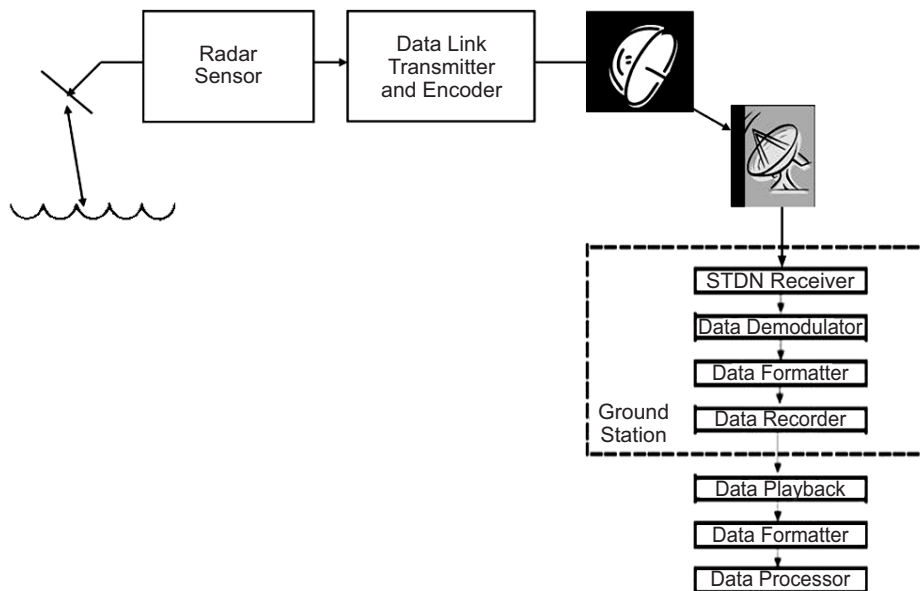


Fig. 6-7. Overall Seasat SAR operation.

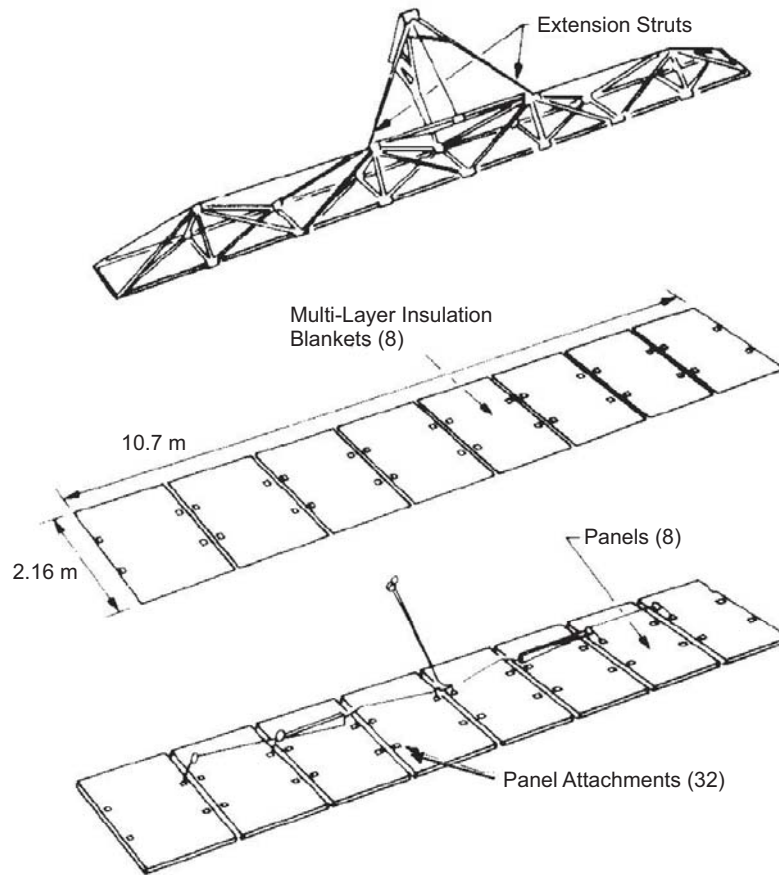


Fig. 6-8. Seasat deployment structure and eight microstrip panels.
The eight panels were mounted on the composite truss structure to be deployed in space.

boresight was at a fixed angle of 20.5 deg from the nadir direction in elevation and 90 deg from the nominal spacecraft velocity vector. As discussed in Section 6.2, the antenna dimensions were set to keep the range or azimuth ambiguities to acceptably low levels. At a nominal 20.5-deg look angle from nadir, the 3-dB beam width required to illuminate the 100-km swath from an 800-km altitude is 6.2 deg. Therefore, the antenna width is 2.16 m. The swath starts from a distance of 240 km from the local nadir on the ground and ends at the far range of 340 km from this nadir point.

To form a coherent antenna beam, eight microstrip panels were fed from a coaxial corporate feed network. The construction of the microstrip panel is depicted in Fig. 6-9, and the overall antenna performance parameters are shown in Table 6-1. A significant factor in the development of this antenna was the

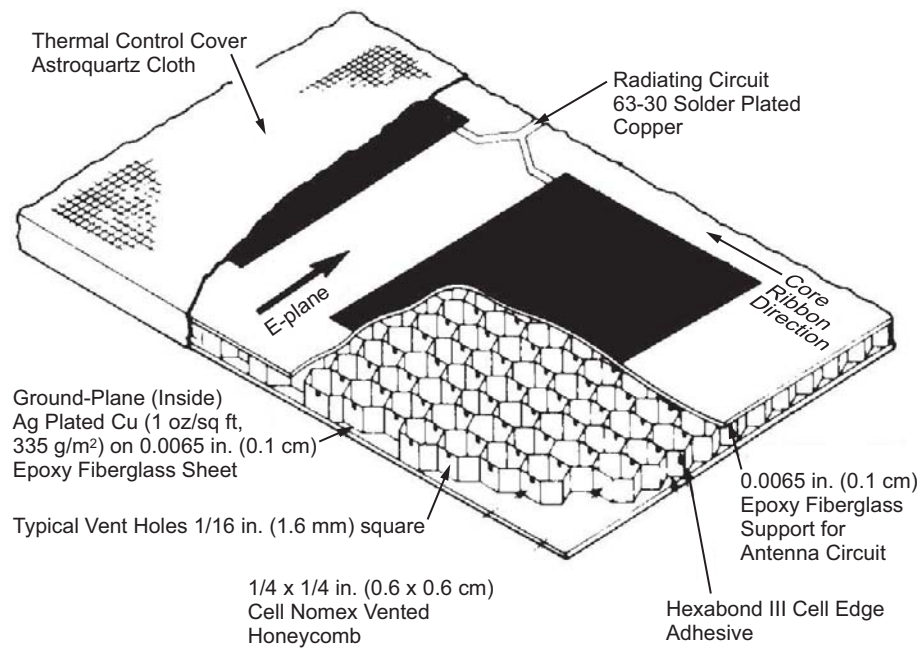


Fig. 6-9. Seasat L-band antenna panel construction using a honeycomb structure.

Table 6-1. Seasat antenna parameters.

Parameter	Value
Radiation gain	37.2 dB
Antenna efficiency	60 percent
Effective gain	35 dB at sensor electronics
Peak power	1100 W (1500 W design)
Beam width in elevation	6.2 deg
Beam width in azimuth	1.7 deg
Polarization	Horizontal polarization
Polarization isolation	20 dB
Center frequency	1.275 GHz
Bandwidth	19 MHz
Peak sidelobe	<-12.5 dB
Phase error in transfer function	±20 deg peak for quadratic error 2 deg rms for random error (higher than quadratic)
Beam pointing	90 deg in azimuth (orthogonal to the flight path) 20.5-deg mechanical tilt in look angle

need to obtain a high overall efficiency between the transmitter and the antenna radiators. The use of conventional coaxial cables for the corporate feed network was ruled out due to high loss, and a corporate feed network using vacuum as the dielectric was developed. This corporate feed network used a solid center conductor in a rectangular structure suspended by solid supports. The total losses introduced by this corporate feed network were less than 1 dB to the individual panels. The Seasat SAR system was designed to use optical processing as the principal method of generating data products on the ground. Optical processors can easily compensate for quadratic phase errors across the frequency spectrum of the transfer function; therefore, a 20-deg maximum quadratic phase error was allowed to be introduced by the antenna. This antenna phase error was removed during the processing step. Since random errors cannot be removed by optical processors, the phase error beyond the quadratic error was limited to 2-deg rms across the frequency spectrum. The Seasat antenna satisfied this phase error requirement.

A photograph of the front surface of the Seasat antenna supported by the strongback is shown in Fig. 6-10(a). A photograph of the back of the Seasat-A antenna supported by the zero-G fixture is shown in Fig. 6-10(b). Figure 6-10(b) shows the truss structure as well as the corporate feed network.

Following the success of the Seasat SAR system, the first of the Shuttle Imaging Radar (SIR) systems, SIR-A, was flown in the Shuttle in 1981. This radar used the residual hardware from Seasat. In particular, the antenna system used seven engineering model (EM) Seasat panels. The antenna was mounted on a fixed structure in the payload bay of the Shuttle and operated at a fixed angle of 50 deg from nadir. The SIR-A hardware was composed of the flight sensor (Seasat flew the engineering model sensor) from Seasat and the spare flight recorder from the Apollo 17 lunar sounder experiment. In 1984, this same antenna was flown on the Shuttle again as the SIR-B antenna.

6.4 SIR-C and SRTM Antennas

The SIR-C/X-SAR mission is a cooperative experiment between NASA, the German Space Agency (DARA), and the Italian Space Agency (ASI). The SIR-C (Shuttle Imaging Radar-C) was launched on the Space Shuttle Endeavor twice in 1994. The SIR-C data have been used to develop algorithms for understanding the global environment and its changes. SIR-C collected radar images over 300 sites around the Earth. These sites were selected to study the focused science in geology, ecology, hydrology, and oceanography. SIR-C generated fully polarimetric radar images at two frequencies (L-band and C-band) while X-band SAR data were acquired by X-SAR provided by DARA and ASI. The SIR-C data were radiometrically calibrated to produce the accurate normalized backscattering cross section of various ground objects for many science applications [12,13].

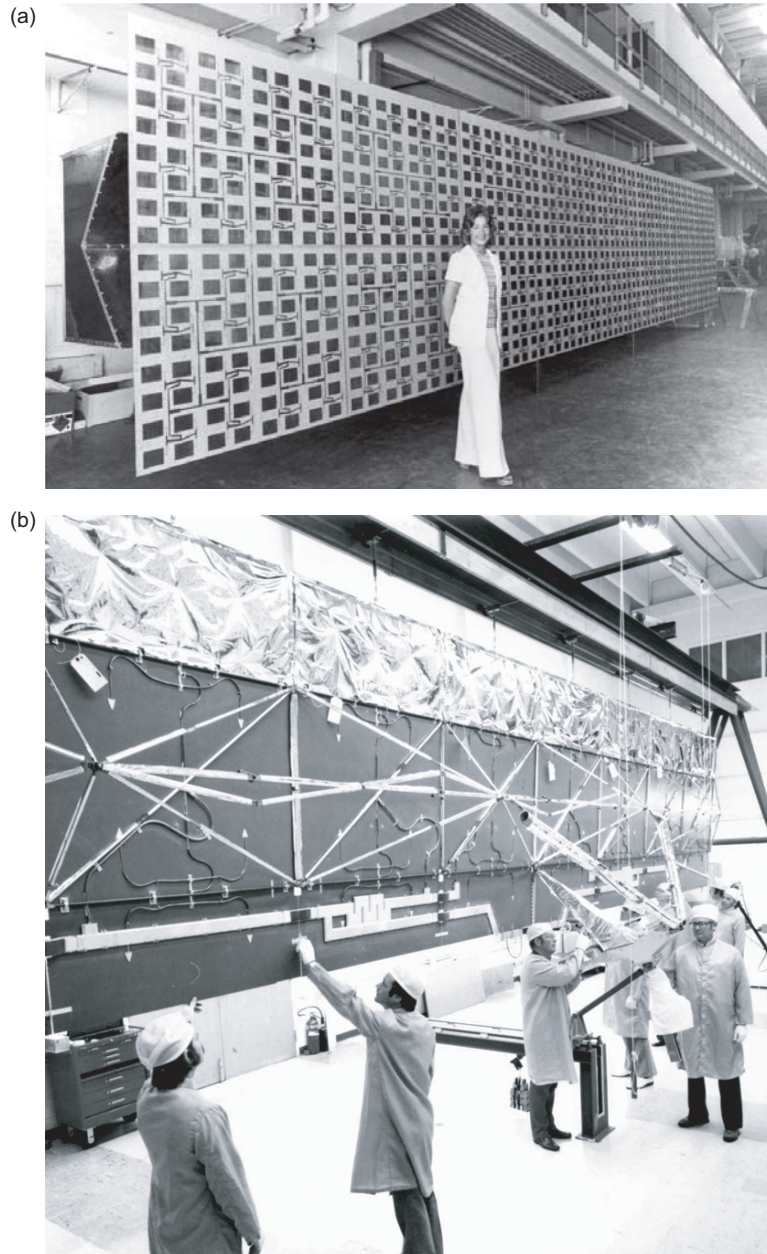


Fig. 6-10. Pictures of Seasat antenna: (a) Front antenna surface (notice that the radiation patches are fed by microstrip feed lines) and (b) back antenna surface (notice that the panels are mounted on a composite truss structure to be deployed in space). All eight microstrip panels are fed from a coaxial corporate feed network.

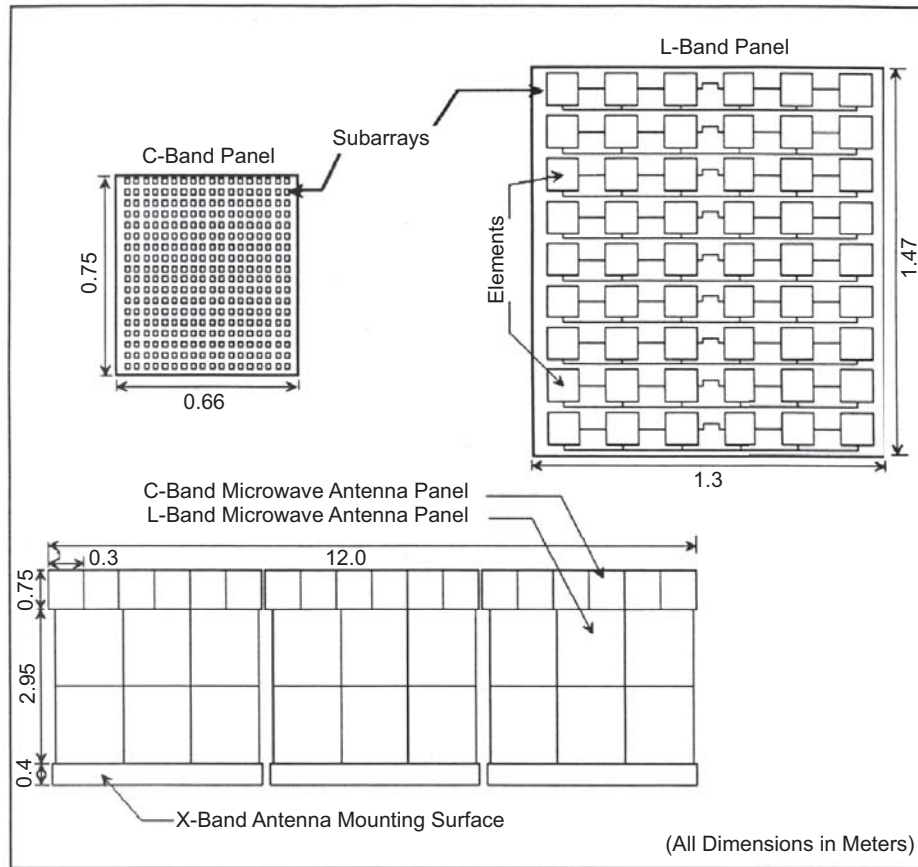


Fig. 6-11. SIR-C antenna configuration. Notice that the L-band phased array in the elevation direction is composed of two panels. Each radiation element is fed by H- and V-polarization feed lines on the front panel surface.

The SIR-C antenna is a dual linear polarized phased array. The antenna was designed and manufactured by Ball Aerospace in close collaboration with JPL. The phased array technology was selected to detect low cross-polarization returns. A phase array is highly efficient since T/R modules are placed close to radiation elements to avoid the feed loss. The SIR-C antenna is composed of 18 L-band panels and 18 C-band panels, as shown in Fig. 6-11. The C-band array size is 12 m by 0.75 m, and the L-band array size is 12 m by 2.95 m. Notice that the array size in the along-track direction is the same for both L- and C-band arrays to use the same PRF. Each L-band panel has nine radiating sticks, and each stick has six radiating elements. Each element is dual linear polarized (horizontal and vertical polarizations). Notice that there are two L-band panels in the cross-track direction. Each C-band panel has 18 sticks, and each stick has 18 radiating elements. Like L-band, a C-band radiating element

is dual polarized. The initial design of the SIR-C system was to occupy one quarter of the shuttle payload bay in its stowed configuration, and the antenna was to be deployed in space. However, during the development phase, it was decided that the antenna would be launched with the deployed configuration.

Using the phase shifters, the antenna beam can be electronically steered in both cross-track and along-track directions. Since there is one phase shifter for each stick, the azimuth steering angle is limited. The required steering angles are within ± 23 degrees in the cross-track direction and within ± 2 degrees in the along-track direction. One L-band panel has 7 T/R modules for each polarization as shown in Fig. 6-12 while one C-band panel has 14 T/R modules. Even though all T/R modules are identical, the arrangement of the antenna electronics, as shown in Fig. 6-12, provides the necessary antenna tapering in the cross-track direction to control the sidelobe level. Two L-band panels (tapering shown in Fig. 6-12 and its mirror image) form the complete elevation tapering, while a single C-band panel has the complete elevation tapering. The

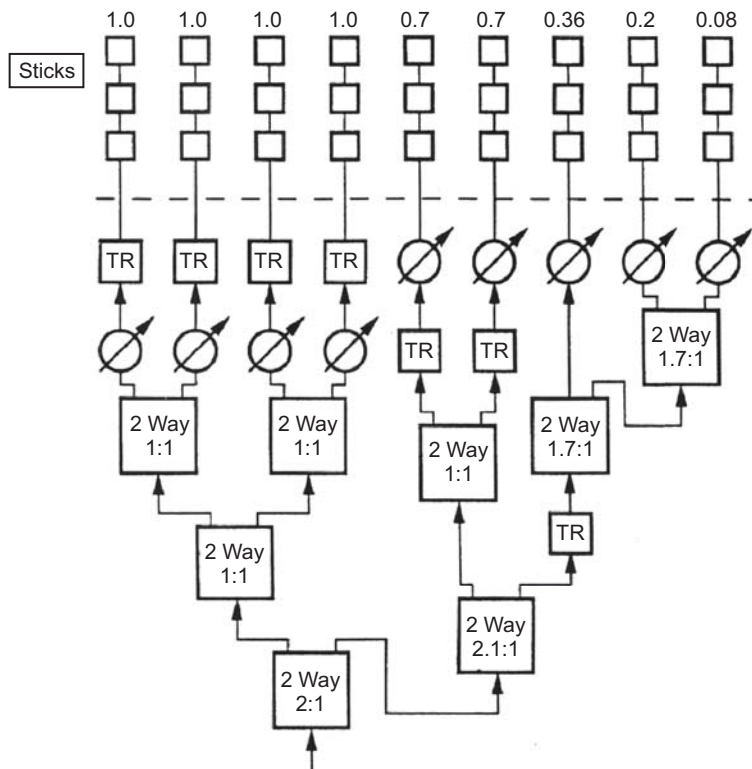


Fig. 6-12. SIR-C elevation tapering obtained by the arrangement of T/R modules, power dividers, and phase shifters. The tapering is given in power, and the amplitude tapering is the square root of the power tapering coefficients.

SIR-C phase shifter is a four-bit p-type–insulator–n-type (PIN) diode phase shifter. The elevation beam width can be changed using the phase tapering (ϕ_T) given by

$$\phi_T(n) = A_{BW} \sin[(n-1)\pi/17] \quad (6.4-1)$$

where A_{BW} takes on 0, 60, 90, 120, 150, 180, 210, or 270 deg, and n is the stick number between 1 and 18. The phase tapering is given in the half cycle of the sine function, and the larger value of A_{BW} provides a broader elevation beamwidth.

In order to calibrate the backscattering measurement accurately, we must be able to predict the SIR-C antenna patterns during the mission based on the pre-launch antenna data. The antenna patterns can be verified during the mission using ground calibration equipments and natural targets, such as rain forests. However, we could not check all the SIR-C antenna patterns due to a large number of possible antenna patterns (two polarizations, elevation steering angles, and various phase taperings). In order to predict the antenna pattern, we tested each panel separately, and the final antenna array performance was computed based on the panel data. The entire array power pattern ($P(\theta, \phi)$) can be calculated by using the stick pattern ($S(\theta, \phi)$) and the array factor given by

$$P(\theta, \phi) = F(\theta, \phi)^2 \quad (6.4-2)$$

and

$$F(\theta, \phi) = S(\theta, \phi) \sum_{n=1}^N \sum_{m=1}^M C(n, m) \exp\left[-j \frac{2\pi}{\lambda} (\cos(\theta) \sin(\phi) d_a(n) + \sin(\theta) d_e(m))\right] \quad (6.4-3)$$

where θ is the elevation angle (cross-track direction), ϕ is the azimuth angle (along-track direction), $d_a(n)$ is the stick locations in the azimuth direction, $d_e(m)$ is the stick locations in the elevation direction, N is the number of sticks in the azimuth direction, and M is the number of sticks in the elevation direction. The elevation stick separation distance is 0.673λ at L-band and 0.696λ at C-band. The stick separation distance in the azimuth direction is 5.58λ at L-band and 11.84λ at C-band, which limits the azimuth steering angle.

In order to estimate the array antenna pattern, we first measured the stick patterns using the far-field measurement facility at Ball Aerospace. Both elevation and azimuth pattern measurements were made for four cases: two frequencies (L- and C-band) and two polarizations (horizontal and vertical). The L-band, H-polarization stick patterns are shown in Fig. 6-13.

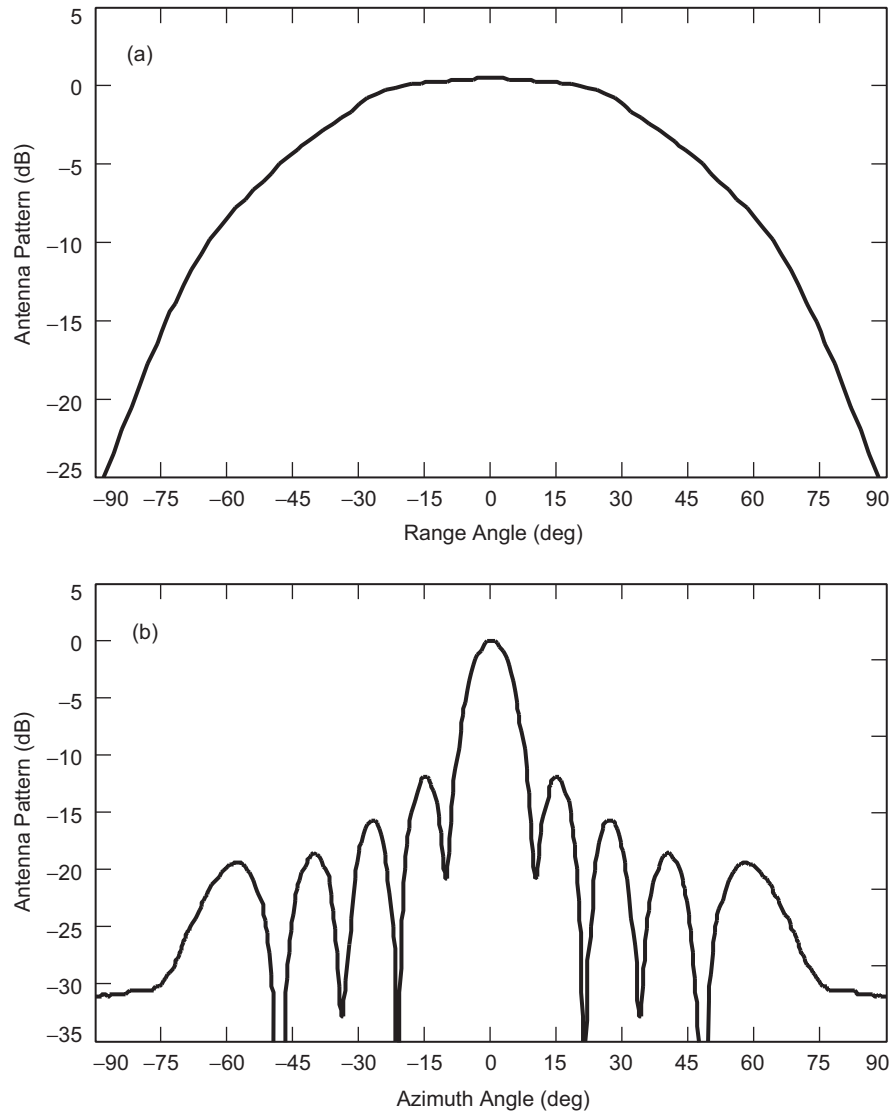


**Fig. 6-13. SIR-C L-band, H-polarization measured stick patterns:
(a) elevation and (b) azimuth.**

As shown in Fig. 6-13, the elevation pattern is the antenna pattern of a single radiation element, and the azimuth pattern is a six element array pattern. The only unexpected stick pattern was the C-band, vertical polarization, elevation pattern (see Fig. 6-14). Two blind zones near ± 25 deg are shown in Fig. 6-14. We conjecture that these blind zones are caused by the surface wave excited by a periodic structure formed within a panel. Notice that the C-band

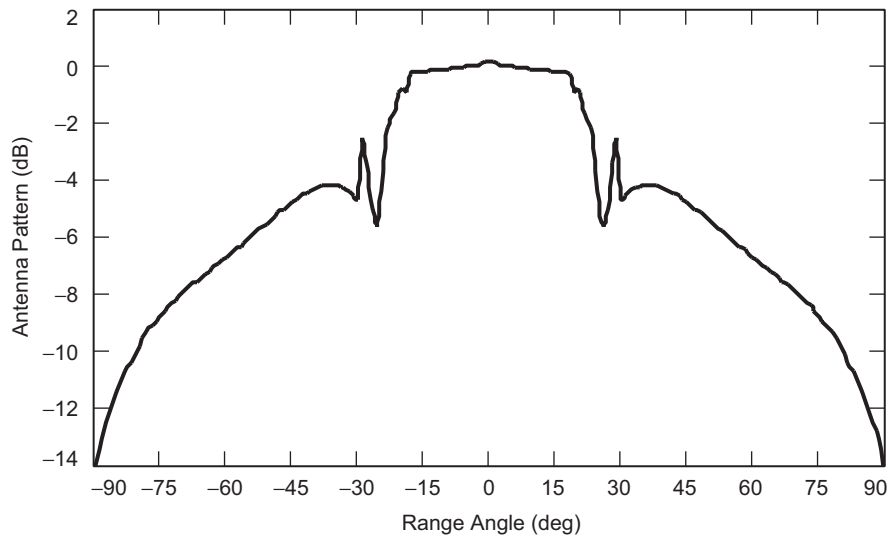


Fig. 6-14. SIR-C C-band, vertical polarization, elevation stick pattern.
Notice that there are blind zones near ± 25 deg.

panel has a high dielectric substrate and the radiating sticks are periodically placed on the panel.

To estimate the entire phase array antenna pattern, we need to measure the complex amplitude ($C(n,m)$) of each stick as shown in Eq. (6.4-3). The complex amplitude includes the amplitude tapering, the path length difference, the phase shifter effect, and other random errors. In order to measure the complex amplitude of each stick, Ball Aerospace developed a “near-field” probe that is almost in contact with each stick of a panel. The manual probe is shown in Fig. 6-15. This manual probe has two coupling elements that can be moved to different sticks; however, an automatic probe was developed later to measure the electromagnetic field of all the sticks in a panel without moving the coupling elements. This probe was originally developed to verify the T/R module functionality by measuring the electromagnetic field of each stick. However, with the probe-calibration technique developed by JPL and Ball, the SIR-C antenna patterns were estimated using the “near-field” probe data and Eq. (6.4-3). We calibrated the probe by comparing far-field pattern measurements with the “near-field” probe data. Using Eq. (6.4-3), one can invert the complex amplitude of each stick from the far-field measurements (amplitude and phase). Then, the ratio of these two stick fields was used to calibrate the probe element associated with each stick location.

The path length difference at the panel level is caused by the feed network and the total path length within a panel. Therefore, all antenna panels were compensated for the path length difference by inserting a phase trimmer to each panel. A separate trimmer was used for the H- and V-polarization port of each

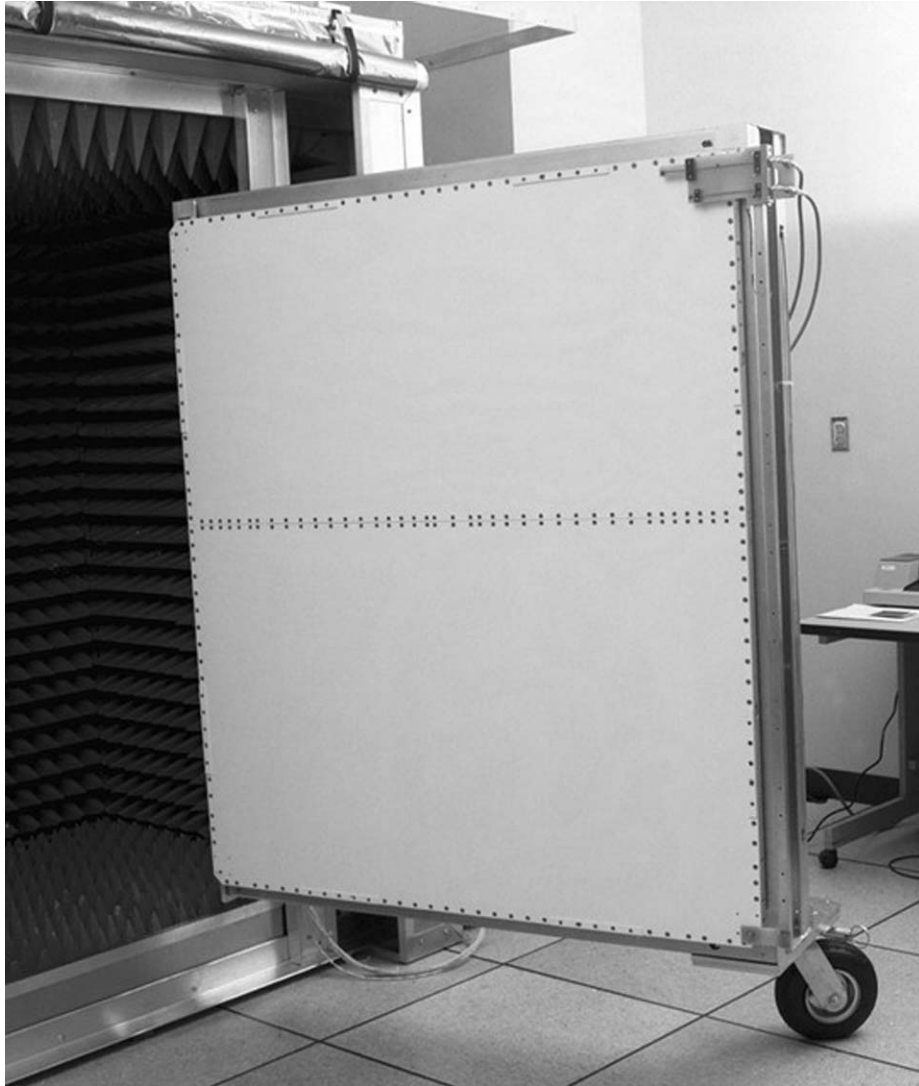


Fig. 6-15. L-band manual "near-field" probe attached to an L-band panel. The "near-field" probe is shown in the right side of the panel. At the top of the panel, two probe-coupling elements for each polarization measure the electromagnetic field of each stick.

panel. The small panel physical location variation was also compensated using the same trimmer. After all the trimmers were installed to the panels, the SIR-C array antenna pattern was estimated using the calibrated probe data as shown in Fig. 6-16. During the mission, these patterns were compared with the ground measurements and the derived patterns using rain forests. The patterns using the

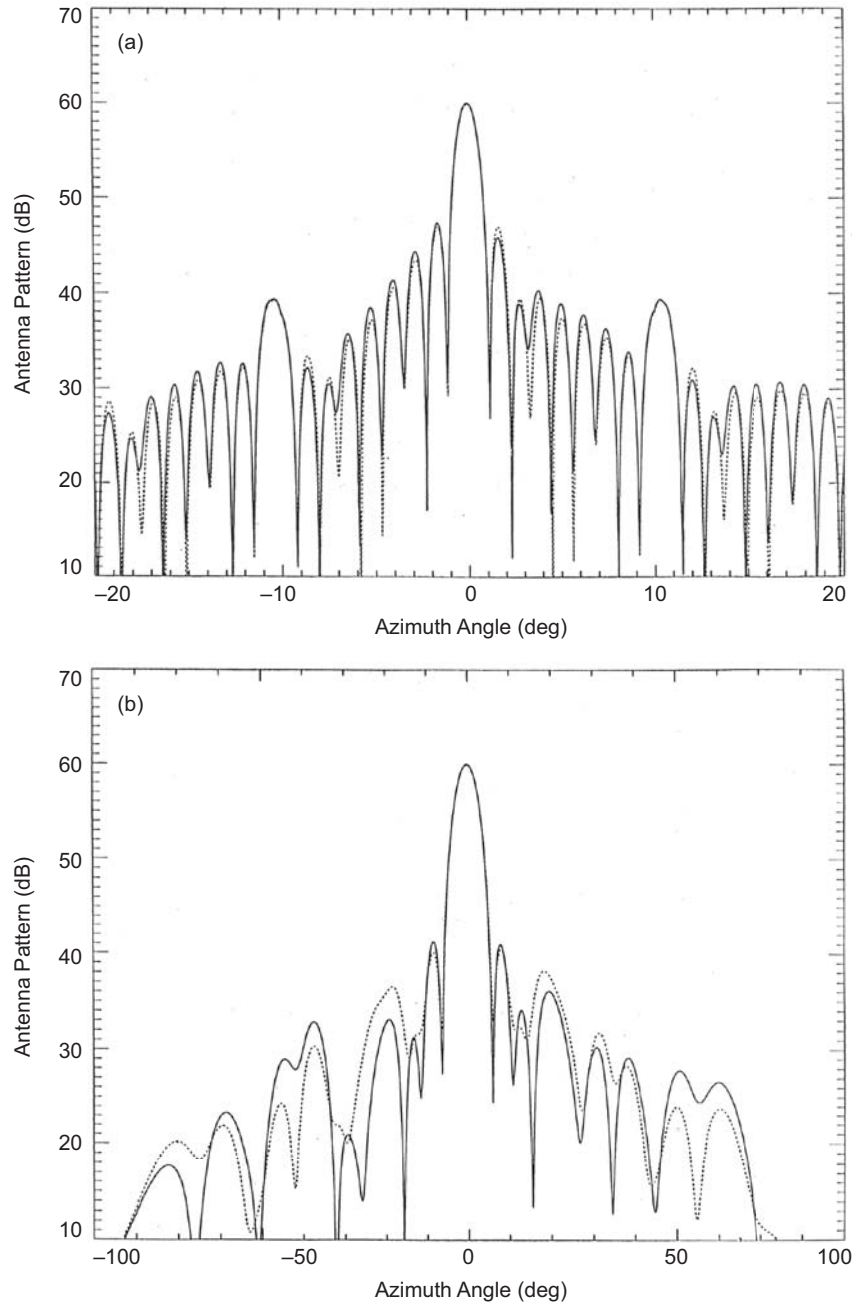


Fig. 6-16. SIR-C L-band, receive antenna patterns for H-polarization: (a) azimuth pattern and (b) elevation pattern. Notice that two patterns are shown in each plot. These two patterns were generated using two probe data sets measured at different times.

probe data compared well with the derived patterns for the low-phase tapering cases. However, for the large-phase tapering cases where the 3-dB beamwidth was significantly broadened, the estimated antenna pattern was not very accurate. During the mission, the health of all T/R modules and phase shifters was also checked using the RF built in test equipment (BITE). The BITE was incorporated into the design of each panel by including a built-in coupler to sample the power going to each of the radiation elements as well as having the ability to inject a known signal into each of the receive modules.

The SIR-C antenna performance was summarized in Tables 6-2 and 6-3. The SIR-C antenna parameters were either directly measured or derived using the analysis. These parameters were evaluated at the room temperature, and their temperature dependences were estimated using limited thermal measurements. For example, the receiver electronic gain was increased as the operating temperature decreases. The receive gain shown in Table 6-2 includes the electronic gain of T/R modules, the total insertion loss, and the antenna directivity. The receive noise temperature of a T/R module is also an important factor in determining SNR. In order to verify that the SIR-C SNR satisfies the requirement, we need to measure antenna related parameters such as EIRP, receive gain, and gain over noise temperature (G/T). The peak sidelobe level is

Table 6-2. Summary of the SIR-C L-band antenna performance.

Parameter	Specification	Performance	Uncertainty (1σ)
EIRP	>102 decibels referenced to mW (dBm)	H: 105.72 dBm V: 104.86 dBm	0.5 dBm
Receive gain	>52.8 dB	H: 57.16 dB V: 57.02 dB	0.5 dB
Polarization isolation	<-25 dB	<-25.24 dB	3 dB
Elevation beam steering accuracy	< ± 0.5 deg	< ± 0.5 deg	0.12 deg
Azimuth beam steering accuracy	< ± 0.1 deg	< ± 0.03 deg	0.014 deg
Elevation peak sidelobe	<-16 dB	<-18 dB	1 dB
Azimuth peak sidelobe	<-12 dB	<-10.36 dB	0.5 dB
G/T	>10.50 (in dB)	10.25 dB (H-polarization) 10.09 dB (V-polarization)	0.6 dB
Impulse response ISLR	<-18 dB	H: -26.43 dB V: -17.86 dB	0.1 dB

H = horizontal; V = vertical

Table 6-3. Summary of the SIR-C C-band antenna performance.

Parameter	Specification	Performance	Uncertainty (1σ)
EIRP	>105.9 dBm	H: 105.81 dBm V: 105.52 dBm	0.5 dBm
Receive gain	>64.2 dB	H: 66.8 dB V: 67.79 dB	0.5 dB
Polarization isolation	<-25 dB	-33.13 dB	0.7 dB
Elevation beam steering accuracy	< ± 0.5 deg	< ± 0.5 deg	0.25 deg
Azimuth beam steering accuracy	< ± 0.1 deg	< ± 0.02 deg	0.0004 deg
Elevation peak sidelobe	<-16 dB	<-12.93 dB	0.8 dB
Azimuth peak sidelobe	<-12 dB	<-11.32 dB	0.4 dB
G/T	>16.50 (in dB)	15.34 dB (H-polarization) 15.40 dB (V-polarization)	0.95 dB
Impulse response ISLR	<-18 dB	H: -25.98 dB V: -27.30 dB	0.1 dB

H = horizontal; V = vertical

related to the range and azimuth ambiguities. Even though the azimuth peak sidelobe level did not satisfy the specification, the SIR-C radar parameters were chosen to keep the azimuth ambiguity less than -20 dB. The time-domain impulse response was characterized by the integrated side-lobe ratio (ISLR) using the antenna frequency transfer function. However, the overall ISLR can be controlled by the range window function during the ground data processing. The transmit spurious signal was measured to be less than -35 decibels referenced to a carrier (dBc) to ensure that the SIR-C antenna did not interfere with other instruments. For a phased array, the voltage standing wave ratio (VSWR) of a panel is not very important since a low-level signal is fed into the panel. The antenna test process was designed to verify the overall radar performance within the budget limitation; therefore, the uncertainty of some parameters was allowed to be large if they were not considered critical to the overall radar performance.

The Shuttle Radar Topography Mission (SRTM) was a joint project between NASA and the National Imagery and Mapping Agency (NIMA). It was the first spaceborne implementation of a single-pass interferometer [14]. A single-pass interferometer measures two interferometric SAR datasets simultaneously using two antennas that form an interferometric baseline. The

SRTM was launched on the Space Shuttle Endeavour in February 2000. The SRTM used the modified SIR-C hardware with a 62-m long mast and a second antenna (known as “outboard antenna”) to form a single-pass interferometer, as shown in Fig. 6-17. The antenna (known as the “inboard antenna”) inside the Shuttle payload bay transmitted a radar signal, and both antennas (inboard and outboard antennas) received the return signal to form an interferogram. During one 11-day Shuttle mission, the SRTM acquired interferometric data between 60 deg north and south latitudes. In order to complete the global coverage within 60 deg north and south latitudes within 11 days, the SRTM implemented a ScanSAR operation to obtain a 225-km swath. JPL finished the global digital elevation model (DEM) production in January 2003, and an example of the SRTM global topographic data is shown in Fig. 6-18.

As shown in Fig. 6-17, the topographic height (z) can be measured using

$$z = H - \rho \cos \theta_L \quad (6.4-4)$$

where H and ρ are the platform altitude and the slant range, respectively. The look angle θ_L is derived from the interferometric phase measurement (ϕ) as

$$\theta_L = \alpha - \sin^{-1} \left[\frac{\lambda \phi}{2\pi B} \right] \quad (6.4-5)$$

where B and α are the baseline length and the tilt angle, respectively. For SRTM, the baseline length, the tilt angle, and the wavelength are 62 m, 60 deg, and 5.6 cm, respectively. It is important to maintain the baseline length between two antennas. That is, the phase centers of both antennas should not vary within the data-take duration since each data-take starts and ends with an ocean data-take that provides the baseline calibration. The failed T/R modules can effectively change the electrical baseline length. However, the final results showed that the phase centers of both antennas did not change within a data-take. The phase noise error of the interferometric system must be less than approximately 15–35 deg (depending upon the location within swath) to meet the vertical accuracy of the SRTM DEM. The stability of the antenna phase and the phase center location are critical factors in achieving the SRTM DEM accuracy. However, this stability is required only between ground control points that can provide the interferometric calibration.

The inboard C-band antenna was the SIR-C antenna, and the outboard antenna was designed and manufactured by Ball Aerospace specifically for SRTM. This outboard antenna is composed of 12 panels, and it is dual polarized. Each panel is 0.75 m \times 0.66 m. The length of the outboard antenna is 8 m, and it is a receive-only antenna. The important consideration in this interferometric antenna system was to overlap two azimuth beams (inboard and outboard azimuth antenna beams) since the azimuth antenna pattern is

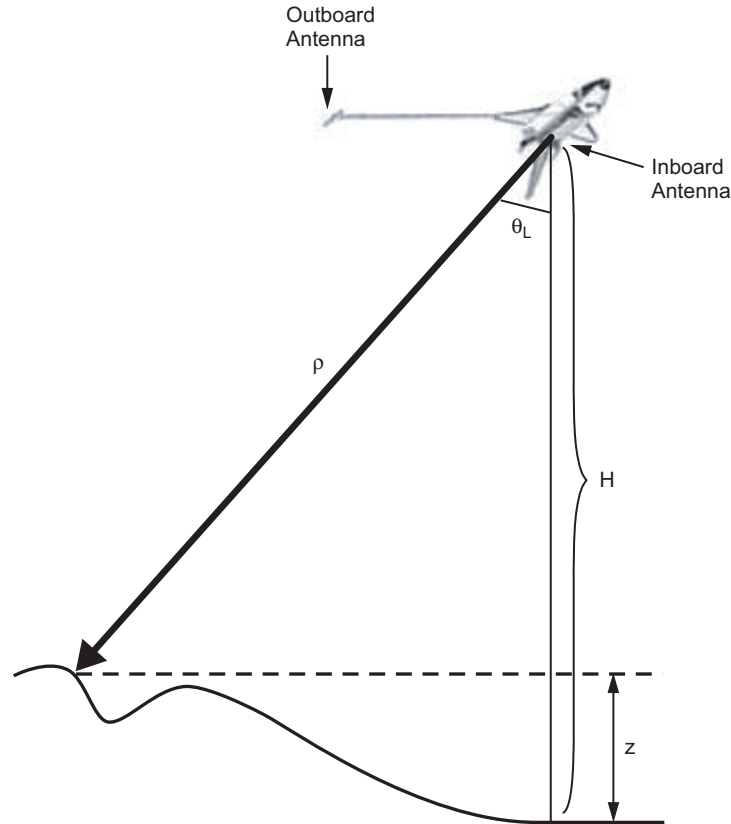


Fig. 6-17. Single-pass interferometric SAR operation. The interferometric phase determines the look angle (θ_L) and the slant range (ρ) is measured by SAR. In addition, the altitude (H) of the platform is estimated by a Global Positioning System (GPS) located near the SAR antenna.

extremely narrow. To insure that both azimuth beams overlap, the outboard antenna length is shorter than the inboard antenna length. The reason that we implemented a shorter outboard antenna instead of a shorter inboard antenna is to maintain the high SNR since the inboard antenna transmits radar signals for both antennas. The electronic scanning capability is ± 20 deg in elevation and ± 0.2 deg in azimuth to implement a ScanSAR operation and to ensure the azimuthal beam overlap. The outboard antenna has a capability of auto-tracking the inboard antenna azimuth beam. The antenna, in addition to electronic scanning, has the capability of increasing its beamwidth in the elevation direction using the phase tapering. Both orthogonal polarizations (horizontal and vertical) operate simultaneously with independent electronic beam steering angles to enable the four-beam ScanSAR operation as shown in Fig. 6-19.

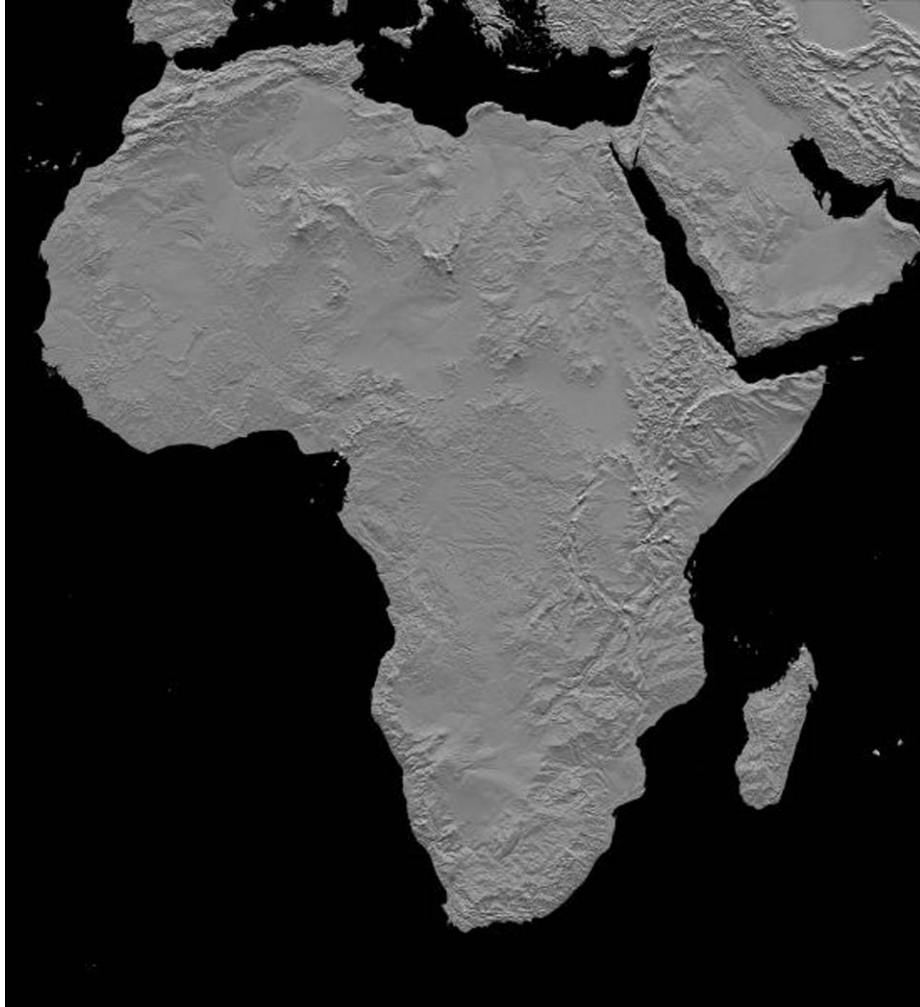


Fig. 6-18. Shaded relief image of Africa's topography measured by SRTM. The post spacing of this DEM is 30 m, and the vertical accuracy is about 7 m.

The radiating element of an outboard panel is identical to that of an inboard panel. For the antenna electronics, each stick has two monolithic microwave integrated circuits (MMIC) receive LNA/phase shifters for horizontal and vertical polarizations. The MMIC LNA/phase shifters are packaged in four modules (quad-receive module) to combine four sticks coherently. These quad-receive modules are combined by a five-way combiner to form the penta-receive module. There are two penta-receive modules (horizontal and vertical polarizations) within a panel. A lightweight panel structure was used to minimize the weight of the outboard antenna that was attached to the end of the

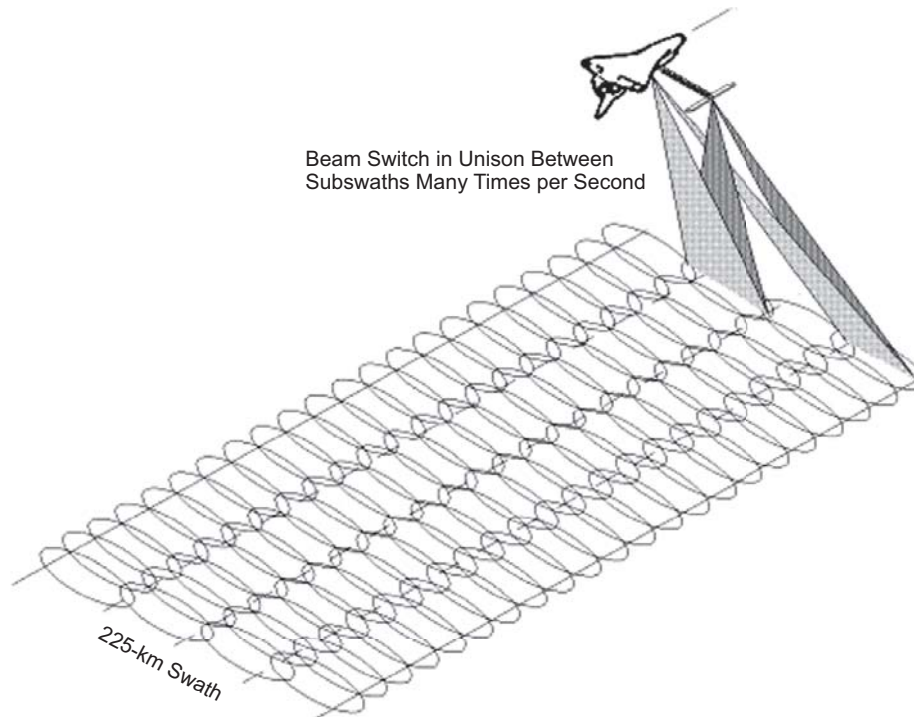


Fig. 6-19. SRTM ScanSAR operation sequence. The near and the far swaths are imaged by the horizontal polarization radar, and the two center swaths are imaged by the vertical polarization radar.

62-m mast. Since the outboard antenna is a receive-only antenna, each panel has two inputs, one for DC power and one for phase shifter commands. In addition, each panel has three outputs, one DC BITE output and two RF outputs (horizontal and vertical polarizations).

The outboard panels were combined by an equal 12-way corporate feed distribution network made up of coaxial cables and microstrip power dividers. Two independent and identical feed networks were used for horizontal and vertical polarizations. The phase balance was maintained between all paths so that the outboard array formed a coherent beam with the required sidelobe level. Unlike SIR-C, phase trimmers were not used to equalize the panel path length. Instead, the phase shifter settings of the outboard antenna were modified assuming that the path length difference does not exceed the wavelength. In order to enable the auto-tracking of two azimuth beams (inboard and outboard antenna beams), two RF signals were coupled from the main corporate feed. The outboard azimuth beam tracked the inboard beam by maximizing the received power of the outboard antenna. The polarization isolation between

horizontal and vertical polarization channels was greater than 25 dB. The steering range in the elevation (cross-track) direction from the mechanical boresight was ± 20 deg with an accuracy of ± 0.25 deg. In addition, the outboard antenna was capable of steering the azimuth beam electronically by ± 0.5 deg in incremental steps less than 0.01 deg.

6.5 Future Antenna Technologies and Concluding Remarks

Future SAR antenna technologies depend strongly upon the antenna size. An important factor in determining the required antenna size is the spacecraft altitude. In order to shorten the revisit time, two different approaches can be implemented: low Earth orbit (LEO) constellation or SAR observations from higher altitudes. The higher altitudes include the medium Earth orbit (MEO) and the geosynchronous orbit. Here, the geosynchronous orbit does not include the geostationary orbit. Geosynchronous orbits have an orbital period equal to one Earth day. The geostationary orbit is a special case since the inclination is zero; therefore, when a satellite in a geostationary orbit is viewed from the rotating Earth, it remains fixed in the same position. Since SAR requires the relative motion between a spacecraft and Earth terrains, geosynchronous orbits will be used for SAR, not the geostationary orbit. For science and applications involved in the solid Earth and natural hazards area, NASA formed the Solid Earth Sciences Working Group (SESWG) composed of senior academic and government scientists to formulate a scientific observational program for NASA. The SESWG final report [15] calls for its highest priority being “InSAR (Interferometric SAR) everywhere, all the time” to make vector surface deformation measurements of mm-scale accuracy over wide areas using the repeat-pass interferometric SAR technology. For the near-term (5–10 years from now) requirement, an InSAR measurement system must provide the capability of daily access to anywhere on the globe. In order to satisfy the long-term (10–25 years from now) requirement, the capability must be increased to hourly global access.

To provide the frequent revisits as required by the SESWG report, a constellation of LEO satellites or higher orbit InSAR satellites are required. An optimum configuration may be a combination of both LEO and higher orbit satellites. For the LEO constellation case, a lightweight antenna with a smaller stowed volume must be developed to lower the overall InSAR life-cycle cost by reducing the capacity requirement on the spacecraft and a launch vehicle. For higher orbit InSAR satellites, a large SAR antenna is required to provide enough SNR.

One new technology that can provide lightweight antennas is an inflatable structure technology. When the inflatable structure technology is combined with the membrane electronics technology, the mass of a SAR antenna can be

reduced dramatically [16]. As an example, a roll-up membrane antenna with an inflatable structure can be stowed within a small volume. When the inflatable structure is fully inflated, the roll-up antenna is deployed to be a fully functional SAR antenna. This antenna can include the active antenna electronics such as membrane T/R modules.

A large SAR antenna technology is composed of structure, electromagnetic radiator, and radar electronics technologies. The large structure technology also includes a metrology system to measure the antenna surface deformation and the compensation method to compensate the effect of a deformed antenna surface. If a large antenna structure is rigid enough, no metrology and compensation technologies are required. The usual SAR antenna deformation that can be tolerated is $1/20$ of the radar wavelength.

6.5.1 Antenna Structure Technology

Since a spaceborne SAR antenna is large, it is important to select the optimum antenna structure technology to reduce the antenna mass and the deployment risk. Due to the large size of a SAR antenna, it is necessary to deploy an antenna in space. For a typical LEO SAR antenna size (10–15 m length and 1–3 m in width), a Seasat-type deployment structure can be used for rigid panels. If a membrane panel technology is developed, an inflatable structure can be used to reduce the antenna weight and the stowed volume. However, the in-space rigidization of an inflatable structure must be demonstrated to ensure the successful deployment. Maintaining the flatness is also an important factor in evaluating the membrane panel technology.

When the antenna size becomes much larger than a typical LEO SAR antenna, the antenna structure technology becomes very complex. If the structure is not rigid enough to maintain the required antenna flatness, the antenna structure must be smart enough to correct the deformation. This is particularly true for the transmit antenna pattern since the transmit pattern must be corrected in real time. There are two methods for correcting the structure deformation in real time: mechanical correction and electrical compensation. The mechanical correction is usually accomplished by actuators, and the electrical compensation is performed using phase shifters or true time-delay elements. The choice of a phase shifter or a true time-delay element depends on the fractional bandwidth required by the SAR operation. In order to use the surface deformation correction, we need to measure the deformation in real time. Therefore, a metrology system must be developed to measure the antenna deformation accurately.

Both inflatable and mechanically deployable structure technologies are viable for very large SAR antennas. An inflatable structure is simple; however, the space inflatable technology is not mature, and the ground testing is much more complex than a mechanically deployable structure. The technology for a

mechanically deployable structure like the SRTM mast has progressed significantly enough to become reliable.

6.5.2 Electromagnetic Radiator Technology

A circular reflector antenna is not an optimum antenna for SAR since SAR requires the elongated antenna shape. If a circular reflector antenna is used, the reflector has to be partially illuminated. Therefore, the surface area is not properly used. In addition, a reflector antenna does not provide the beam agility. In order to steer the antenna beam, the reflector must be mechanically tilted, or the beam steering angle is limited, even with complex feeds. A cylindrical reflector with a phased array feed is a better candidate for SAR. This design is a compromise between a reflector antenna and a phased array. The phased array feed usually uses the microstrip radiator technology to steer an antenna beam. A reflectarray uses a reflecting surface composed of microstrip radiating elements instead of using a solid reflector. Phase shifters can be included in the radiating element of a reflectarray.

A phased array provides many important characteristics required by SAR, especially if beam agility is required. In order to reduce the antenna weight, membrane microstrip radiators can be used. To feed the membrane microstrip radiators, a multi-layer feed structure can be implemented. A radiator design comparable to lightweight structures needs to be developed to advance the phased array technology.

6.5.3 Antenna Electronics Technology

The antenna electronics include T/R modules, phase shifters, and RF/power/command distribution network. A high-efficiency T/R module needs to be developed to lower the DC power consumption. The Class E type high power amplifier (HPA) is a promising technology, especially at lower frequencies. A low-loss phase shifter is also a critical component if beam agility is needed. The micro electromechanical system (MEMS) RF switch can provide a low insertion loss for a phase shifter. The T/R module and phase-shifter packaging is also important to reduce the weight and complexity of the antenna electronics. The distribution network for RF signal, DC power, and commands must be simplified to be comparable with lightweight structures and the associated deployment mechanism. An optical-fiber distribution network is a promising future technology. The concept of a fully functional panel (including radar electronics) is being considered for an extremely large phased array antenna.

We described the spaceborne SAR antennas for Earth science applications. The planer array technology was used for earlier missions such as Seasat, SIR-A, and SIR-B. Following the success of these SAR missions, a major advancement was accomplished by the SIR-C antenna. The SIR-C antenna was

the first spaceborne, fully polarimetric, phased array antenna. By adding another antenna, the SIR-C hardware was modified to be the world's first single-pass interferometric SAR. The spaceborne SAR antenna is the most critical component to reduce the mass, stowed volume, and cost of a spaceborne SAR. Various new technologies are being developed to enable future spaceborne SAR antennas.

References

- [1] R. L. Jordan, "The Seasat-A Synthetic Aperture Radar System," *IEEE Journal of Oceanic Engineering*, vol. OE-5, no. 2, pp. 154–164, April 1980.
- [2] C. Elachi, T. Bicknell, R. L. Jordan, C. Wu, "Spaceborne Synthetic-Aperture Imaging Radars: Applications, Techniques and Technology," *Proceedings of IEEE*, vol. 70, no. 10, pp. 1174–1209, October 1982.
- [3] E. R. Stofan, D. L. Evans, C. Schmullius, B. Holt, J. J. Plaut, J. van Zyl, S. D. Wall, and J. Way, "Overview of Results of Spaceborne Imaging Radar-C, X-Band Synthetic Aperture Radar (SIR-C/X-SAR)," *IEEE Transactions Geoscience and Remote Sensing*, vol. 33, no. 4, pp. 817–828, July 1995.
- [4] R. L. Jordan, B. L. Huneycutt, and M. Werner, "The SIR-C/X-SAR Synthetic Aperture Radar System," *IEEE Transactions on Geoscience Remote Sensing*, vol. 33, no. 4, pp. 829–839, July 1995.
- [5] T. G. Farr and M. Kobrick, "The Shuttle Radar Topography Mission: A Global DEM," *EUSAR 2000*, VDE-Verlag, Frankfurt am Main, Germany, pp. 41–42, 2000.
- [6] *Shuttle Radar Topography Mission*, web site at Jet Propulsion Laboratory, Pasadena, California, accessed July 26, 2005.
<http://www2.jpl.nasa.gov/srtm/>
- [7] *Living on a Restless Planet*, web site at Jet Propulsion Laboratory, Pasadena, California, accessed July 26, 2005.
<http://solidearth.jpl.nasa.gov/seswg.html>
- [8] J. C. Curlander and R. N. McDonough, *Synthetic Aperture Radar Systems & Signal Processing*, Wiley & Sons, New York, New York, 1991.
- [9] C. Elachi, *Spaceborne Radar Remote Sensing: Applications and Techniques*, IEEE Press, Piscataway, New Jersey, 1988.
- [10] F. M. Henderson and A. J. Lewis, *Principles & Applications of Imaging Radar*, Wiley & Sons, New York, New York, 1998.

- [11] J. J. van Zyl and Y. Kim, "Synthetic Aperture Radar," *Encyclopedia of Physical Science and Technology*, Third Edition, Vol. 16, Academic Press or Elsevier Inc., Burlington, Massachusetts, pp. 451–465, 2002.
- [12] J. J. van Zyl, "Calibration of Polarimetric Radar Images Using Only Image Parameters and Trihedral Corner Reflector Responses," *IEEE Transactions on Geoscience and Remote Sensing*, vol. 28, no. 3, pp. 337–348, May 1990.
- [13] A. Freeman, M. Alves, B. Chapman, J. Cruz, Y. Kim, S. Shaffer, J. Sun, E. Turner, and K. Sarabandi, "SIR-C Data Quality and Calibration Results," *IEEE Transactions of Geoscience and Remote Sensing*, vol. 33, no. 4, pp. 848–857, July 1995.
- [14] H. Zebker and R. Goldstein, "Topographic Mapping from Interferometric SAR Observations," *Journal of Geophysical Research*, vol. 91, pp. 4993–4999, 1986.
- [15] *Living on a Restless Planet: Solid Earth Sciences Working Group Report*, JPL 400-1040, Jet Propulsion Laboratory, Pasadena, California, November 2002, also at web site accessed August 30, 2005. http://solidearth.jpl.nasa.gov/PDF/SESWG_final_combined.pdf
- [16] J. Huang, M. Lou, A. Feria, and Y. Kim, "An Inflatable L-band Microstrip SAR Array," *IEEE Antennas and Propagation Society International Symposium* (Atlanta, Georgia), pp. 2100–2103, June 1998.